Chemical Science

ROYAL SOCIETY OF CHEMISTRY

EDGE ARTICLE

View Article Online
View Journal | View Issue

Cite this: *Chem. Sci.*, 2020, **11**, 7438

All publication charges for this article have been paid for by the Royal Society of Chemistry

Asymmetry controlled dynamic behavior of autonomous chemiluminescent Janus microswimmers†

Gerardo Salinas, Alice L. Dauphin, Silvia Voci, Laurent Bouffier, Neso Sojic * and Alexander Kuhn *

Received 29th April 2020
Accepted 27th June 2020

DOI: 10.1039/d0sc02431g

rsc.li/chemical-science

Asymmetrically modified Janus microparticles are presented as autonomous light emitting swimmers. The localized dissolution of hybrid magnesium/polymer objects allows combining chemiluminescence with the spontaneous production of H_2 bubbles, and thus generating directed motion. These light-emitting microswimmers are synthesized by using a straightforward methodology based on bipolar electromilling, followed by indirect bipolar electrodeposition of an electrophoretic paint. An optimization of the experimental parameters enables in the first step the formation of well-defined isotropic or anisotropic Mg microparticles. Subsequently, they are asymmetrically modified by wireless deposition of an anodic paint. The degree of asymmetry of the resulting Janus particles can be fine-tuned, leading to a controlled directional motion due to anisotropic gas formation. This autonomous motion is coupled with the emission of bright orange light when $Ru(bpy)_3^{2+}$ and $S_2O_8^{2-}$ are present in the solution as chemiluminescent reagents. The light emission is based on an original process of interfacial redox-induced chemiluminescence, thus allowing an easy visualization of the swimmer trajectories.

Introduction

Nowadays self-propelled microswimmers are of importance,[1–9] due to their potential applications in sensing,[10–13] biomedicine[14–16] or environmental remediation.[17,18] In this context, an interesting concept is the design of swimmers that couple mechanical motion and light emission, which enables or facilitates their tracking in real time. Recently, light emitting dynamic systems made out of luminescent materials[19,20] or based on microelectronics (LEDs) have been described.[21–25] In these cases, bubble propulsion or electrokinetic mechanisms cause mechanical motion, whereas photon emission is ensured either by the intrinsic composition of the luminescent object under illumination or by a local voltage difference generated at the poles of the electronic devices. A promising alternative approach to design light-emitting swimmers is based on the use of electrochemiluminescence (ECL).[26] ECL is a light emitting phenomenon, which is triggered by an initial electron transfer reaction occurring at the electrode/solution interface.[27–29] The produced intermediates undergo a homogeneous chemical reaction that leads to the generation of the excited state of the luminophore, which produces light emission after its relaxation to the ground state. ECL is by nature an interfacial process requiring the polarization of the electrode surface either with a direct electrical connection[30] or in a wireless manner with external feeder electrodes[31–33] using bipolar electrochemistry (BE). Different types of dynamic light emitting devices, coupling ECL emission and mechanical motion have already been reported.[26,34–38] In these systems motion can be easily tracked with the naked eye or a simple camera. Moreover, these approaches can be used as sensing and screening devices, due to the electric coupling between the two sides of the swimmer, allowing the design of dynamic systems for bioanalytical applications.[35] Although directional motion can be achieved, either as vertical propulsion or rotation, an input of external power in the form of an electric or magnetic field is needed. Therefore, the challenge to design truly autonomous self-propelled chemiluminescent (CL) swimmers remains. Recently, our group proposed CL biopolymer particles showing oscillatory vertical motion due to an asymmetric character induced by using BE.[39] However, an external chemical fuel (H_2O_2) is necessary to generate motion. Here, for the first time, we report completely autonomous CL swimmers, which need neither addition of fuel nor external electrodes.

BE is an interesting and simple approach to break the symmetry of conducting and semiconducting objects.[40–44] When a conducting object is exposed in solution to an external electric field (ε), applied between two feeder electrodes, a polarization

Univ. Bordeaux, CNRS UMR 5255, Bordeaux INP, Site ENSCBP, 33607 Pessac, France. E-mail: sojic@enscbp.fr; kuhn@enscbp.fr

† Electronic supplementary information (ESI) available: Experimental section, schemes of the electrochemical cells and optical pictures of different Mg particles. Video S1 showing motion of an anisotropic Mg/EP Janus swimmer. Video S2 showing motion of an isotropic Mg/EP Janus swimmer. Video S3 showing motion of a fully isotropic Mg swimmer. See DOI: 10.1039/d0sc02431g

potential difference (ΔV) is generated between the extremities of the object. It can be calculated as $\Delta V = \varepsilon \times d$, where d is the characteristic size of the conducting object along the electric field lines. In the presence of electroactive species, redox reactions can occur at both extremities of the object, which behaves as a bipolar electrode (BPE), as long as the polarization potential difference exceeds the thermodynamic threshold required to trigger both reactions (ΔV_{min}). This concept has been already used for the design of microswimmers based on hybrids such as carbon microtubes/Pt,[45] carbon tubes/Ni,[46] polyaniline/alginate[47] and Zn/electrophoretic paint (EP).[48]

In this work, we describe a straightforward methodology to design asymmetrically modified magnesium microparticles using a combination of two different BE processes (Scheme 1a and b): bipolar electromilling[49] for shaping the particle and indirect bipolar electrodeposition for the subsequent asymmetric modification.[48] The resulting Janus objects are simultaneously moving and emitting light by exploiting the redox reactivity of a strong reducing agent (Mg) at the metal/liquid interface (Scheme 1c). Indeed, this redox feature allows triggering both, light emission by generating the excited state $Ru(bpy)_3^{2+}$* and the autonomous propulsion of the microswimmers by the spontaneous formation of H_2 bubbles. Magnesium has already been successfully used to drive micromotors for biomedical and environmental applications.[50,51] The swimmers reported here are based on an intriguing light emitting principle at the frontiers between ECL and CL. Indeed, the light emission results from the initial electron-transfer reactions at the metal/solution interface. In other words, at first sight it resembles an ECL process since the Mg material can be considered as an electrode in an open-circuit configuration. In addition, the interfacial nature of the operating principle estranges it from CL, which normally is a bulk process where the reagents are usually mixed homogeneously. However, the process clearly does not involve any electrode driven by a power supply (neither in a wired nor a wireless mode), which usually defines the ECL phenomenon. Thus, the light emission described herein shares some features specific to ECL and some characteristics of CL. Consequently, we may define it as interfacial CL.

Results and discussion

Bipolar electrochemical milling of magnesium wires

As the goal of this work is to reveal the correlation between the shape/degree of asymmetry of different swimmers and their respective trajectories, it was necessary to fine tune their length and shape. Thus, in order to obtain Mg particles with reproducible features, *i.e.* a desired length and smooth edges, bipolar electromilling has been employed. Bipolar electromilling of magnesium wires was performed following a concept proposed in previous work.[49] The process is based on the asymmetric electrodissolution of a metal, triggered by the polarization of a randomly rotating BPE in an external electric field. This leads to the electrodissolution of the metal (M) as the anodic reaction, whereas reduction of protons is the cathodic reaction, as described in eqn (1).

$$M + 2H^+ \rightarrow M^{2+} + H_2 \quad (1)$$

The ΔV_{min} required to trigger the electrodissolution is governed by the thermodynamics of the global redox reaction. For metals with a non-spontaneous global reaction (*i.e.* copper, $\Delta G^\circ = +65.62$ kJ mol^{-1}), electric fields are required to drive the reaction. However, in the case of magnesium ($\Delta G^\circ = -451.6$ kJ mol^{-1}), reaction 1 occurs spontaneously and therefore, at first sight, no external electric field is needed. We nevertheless applied a low ε value (15 V cm^{-1}) in order to better control the electrodissolution rates of the initially anisotropic metal rods.

Bipolar electromilling of several magnesium wires ($l = 1.2 \pm 0.2$ mm) was carried out under constant stirring in a 5 mM H_2SO_4/ethanol solution. The cell is shown in Scheme S1a.† At

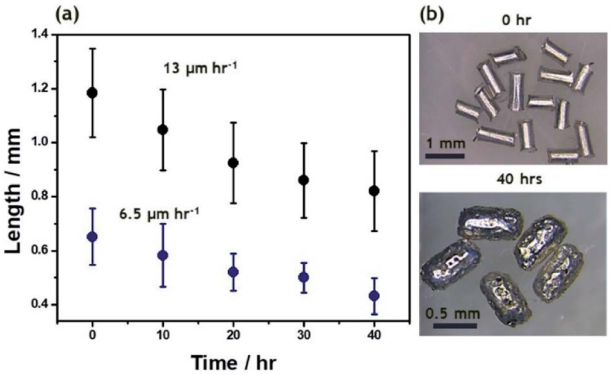

Fig. 1 (a) Average length of Mg wires as a function of electrolysis time at constant $\varepsilon = 15$ V cm^{-1}, for two different initial sizes: 1.2 ± 0.2 mm (black dots) and 0.6 ± 0.1 mm (blue dots). (b) Optical pictures of Mg wires with an initial length of 1.2 ± 0.2 mm before and after 40 h of electrolysis in a 5 mM H_2SO_4/ethanol solution.

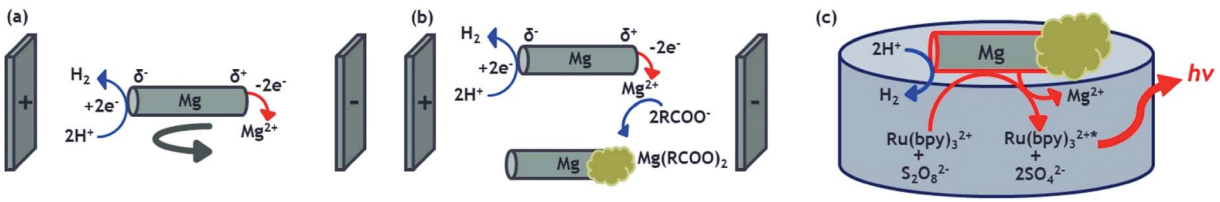

Scheme 1 (a) Illustration of the bipolar electrochemical milling process, (b) mechanism of the indirect bipolar electrodeposition of anodic electrophoretic paint and (c) motion and light emission principle of a self-propelled CL microswimmer.

this low ε value a continuous slow decrease of the average length as a function of the electrolysis time was observed (Fig. 1). After 40 h of electrolysis, the obtained anisotropic Mg microparticles have an average length of 0.8 ± 0.2 mm and a porous surface (Fig. S1†).

In order to obtain Mg particles with an isotropic shape, bipolar electromilling of magnesium wires with a smaller initial length (l = 0.6 ± 0.1 mm) was carried out under the same conditions. As expected, after 40 h of electrolysis, more isotropic Mg particles, with an average dimension of 0.4 ± 0.1 mm, were obtained (Fig. S2†). In the beginning of the milling process, dissolution rates are proportional to the initial size of the Mg wires (13 μm h^{-1} and 6.5 μm h^{-1}, respectively). For longer electrolysis times, the kinetics slows down since the polarization potential difference is proportional to the size of the particles. This approach allows tuning not only the microparticle size, but also the shape, which should affect the resulting motion of the swimmers. From the obtained anisotropic and isotropic particles, the smallest ones were selected for the asymmetric modification by indirect bipolar electrodeposition of an anodic EP.

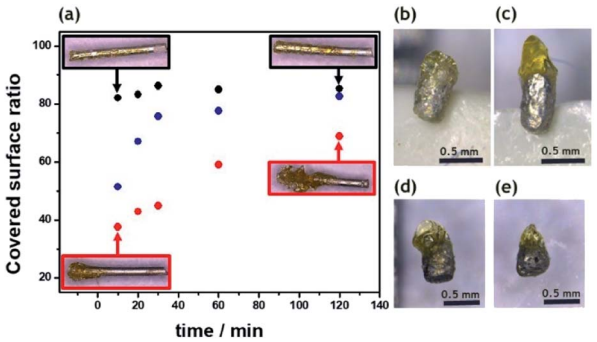

Fig. 2 (a) Covered surface ratio of 5 mm-long Mg wires as a function of electrolysis time at different applied ε: 0.5 V cm^{-1} (black dots), 1 V cm^{-1} (blue dots) and 2 V cm^{-1} (red dots). Inset: optical pictures of the asymmetric deposits of electrophoretic paint (EP) using an ε of 0.5 V cm^{-1} (black frames) and 2 V cm^{-1} (red frames) for 10 and 120 min, respectively. Optical pictures of Mg particles after asymmetrical modification in an electrophoretic paint/water solution (1 : 10) at different ε values and deposition times; (b) 4 V cm^{-1}, 20 min, (c) 6 V cm^{-1}, 20 min, (d) 6 V cm^{-1}, 10 min and (e) 6 V cm^{-1}, 5 min.

Asymmetric modification of microscale magnesium objects

In order to induce directional motion, the symmetry of the obtained Mg microparticles needs to be broken, either through modifying the particle composition, its shape or by changing the local surface reactions.[52] In this work, we use indirect bipolar electrodeposition of an EP, in analogy to what has been previously reported.[48,53] The anodic water-soluble EP selected for this study, presents negatively charged carboxyl groups along the polymer backbone. Fattah *et al.* used the complexation of these carboxyl groups for the precipitation of the polymer at the BPE surface by electrodissolution of metallic Zn.[48] In order to evaluate the influence of the applied electric field and the deposition time, a 5 mm long Mg wire was placed between the feeder electrodes in an EP solution. The used cell is shown in Scheme S1b.† As expected, increasing the ε value increases the polarization of the BPE, which enhances the localized Mg dissolution and consequently allows a targeted EP deposit (Fig. 2a). As the deposition time increases, the EP covers more than 50% of the Mg surface for all the ε values tested. This is due to a competition between the spontaneous redox reaction of Mg and H_2O, which in principle can occur everywhere on the wire, and the side-selective cathodic protection of one extremity of the wire by the applied electric field. Actually, when only a weak or no electric field is applied, almost the whole object is covered spontaneously with paint due to the thermodynamically favorable dissolution of the metal, as illustrated by the Mg wires in the black frames in Fig. 2a. When a sufficiently high electric field is applied, the magnesium dissolution at the anodic extremity is coupled to the reduction of protons at the opposite end. Therefore, the latter extremity benefits from a cathodic corrosion protection, clearly visible on the two wires in the red frames of Fig. 2a.

However, as a function of time, the anodic extremity gets covered with EP, thus converting this section of the wire into an insulator which can no longer participate in the bipolar process. As a consequence, the efficient length of the object, responsible for the polarization in the electric field, is getting shorter. This leads to a constant decrease in driving force for the cathodic reaction, and ultimately to a value of polarization potential difference falling below the threshold, which allows corrosion protection at the cathodic side. Therefore, all wires, almost independent of the initially applied electric field, end up showing similar surface coverages of polymer. Hence, in order to obtain a localized deposit at the tip of the BPE, higher ε values (>2 V cm^{-1}) and short deposition times (<20 min) are required. The same tendency is also observed for Mg microparticles. As can be seen in Fig. 2b, at low ε values the electrodeposition occurs almost all along the particle surface, since the ΔV is not high enough to allow cathodic corrosion protection at one extremity of the BPE. However, an applied ε of 6 V cm^{-1} is enough to polarize the microparticles sufficiently to prevent Mg dissolution at one end and thus leads to localized precipitation of the EP (Fig. 2c). The same concept was also used for the asymmetric modification of isotropic Mg particles (Fig. S2c†). The particles present a localized and well-defined EP deposit, obtained with shorter deposition times compared to the anisotropic ones (<10 min) (Fig. 2d and e). Isotropic particles have a spherical shape, anisotropic particles have a rod like shape and after modification with EP they become Janus particles. As a result, four categories of particles were studied with respect to their performance as self-propelled CL swimmers: isotropic, anisotropic, isotropic Mg/EP Janus and anisotropic Mg/EP Janus particles.

Chemiluminescent microswimmers

Motion of the different particles was probed on the interface of a 1 mM $Ru(bpy)_3(PF_6)_2$, 20 mM $K_2S_2O_8$, 20 mM H_2SO_4 in H_2O/ACN (1/1) solution. Under these experimental conditions, the involved redox reactions are powering two different processes:

the light emission by means of a CL process and the mechanical propulsion *via* the generated hydrogen bubbles. Magnesium acts as a strong reductant, which produces in the presence of $Ru(bpy)_3^{2+}$ and $S_2O_8^{2-}$ the excited state $Ru(bpy)_3^{2+}$*, following a reductive-oxidation ECL-like mechanism.[54,55]

$$2Ru(bpy)_3^{2+} + Mg \rightarrow 2Ru(bpy)_3^{+} + Mg^{2+} \quad (2)$$

$$2S_2O_8^{2-} + Mg \rightarrow 2SO_4^{2-} + 2SO_4^{-\cdot} + Mg^{2+} \quad (3)$$

$$Ru(bpy)_3^{+} + S_2O_8^{2-} \rightarrow Ru(bpy)_3^{2+} + SO_4^{2-} + SO_4^{-\cdot} \quad (4)$$

$$Ru(bpy)_3^{+} + SO_4^{-\cdot} \rightarrow Ru(bpy)_3^{2+}* + SO_4^{2-} \quad (5)$$

The relaxation of the excited $Ru(bpy)_3^{2+}$* to the ground state is accompanied by the emission of a photon with a characteristic wavelength ($\approx$620 nm).

In addition to these reactions, mechanical motion is achieved by the spontaneous oxidation of Mg and reduction of H^+ to form H_2 bubbles at the surface of the metal particle (eqn (6)).[11,15,56]

$$Mg + 2H^+ \rightarrow Mg^{2+} + H_2 \quad (6)$$

As it can be seen, all these reactions are strongly related to the consumption rate of magnesium, due to the high concentration of $S_2O_8^{2-}$ and H^+. Thus in this experiment Mg acts as the limiting fuel in the propulsion mechanism as well as for light emission. It is also noteworthy that the concentration of persulfate should be chosen carefully. Indeed, this sacrificial coreactant is crucial to promote CL. However, it is also known to quench the excited state of $Ru(bpy)_3^{2+}$ at concentrations larger than 20 mM.[54]

Autonomous motion of all swimmers was monitored by video-macroscopy recordings of their light emission. Anisotropic Mg/EP Janus swimmers show a very well defined linear motion at the 2-dimensional air/water interface (Fig. 3a and b and Video S1†), compared to the unmodified isotropic Mg particles, which move in a completely erratic way (Fig. 3c). The partial modification of the Mg microparticles with polymer causes an asymmetric production of H_2 bubbles with respect to the particle axis, resulting in linear motion. In order to evaluate this important effect of particle asymmetry on the directionality of the motion in a more quantitative way, a straightness index was calculated. It is defined by the ratio of the distance (D) between the end and starting point of the trajectory, and the total path length (L).[57] Since this value ranges between 0 and 1, it allows to distinguish random ($D/L < 0.5$) and linear motion ($D/L \approx 1$). The polymer modified anisotropic Mg/EP Janus particles, which have the highest degree of asymmetry of all the studied swimmers, present a straightness index of 0.97 ± 0.04, which is roughly four times higher than the straightness index obtained for an unmodified particle ($D/L = 0.26$). This clearly demonstrates that the proposed methodology allows for the first time designing on purpose CL swimmers with a reproducible and predictable directional motion. An additional very interesting observation is that when reusing the same swimmer for several experiments, the straightness index starts to decrease. For example, a swimmer with an initial D/L value close to one loses 15% of straightness index after five runs ($D/L = 0.83$, Fig. 3d). This can be explained by the gradual and somewhat irregular spatial consumption of Mg, which impacts the symmetry of hydrogen production on the metal surface.

Finally, it is worth mentioning that the intensity of emitted light can be also controlled. Compared to Fig. 3a, the experiment reported in Fig. 3b has been performed with a solution containing less acetonitrile due to slow evaporation. As a consequence, the ruthenium cation, whose charge is compensated by PF_6^- counteranions, is less soluble and thus less $Ru(bpy)_3^{2+}$ luminophore is available for CL emission, leading to a significant decrease in light intensity. The decrease of light intensity is also correlated with the amount of available Mg. The inset of Fig. 3d shows a swimmer after five consecutive runs, indicating that there is much less metal left compared to the beginning (Fig. 3a) and this explains also the lower light intensity recorded during this run. Under the same experimental conditions, Janus swimmers based on initially isotropic Mg particles exhibit in the beginning also a quite linear

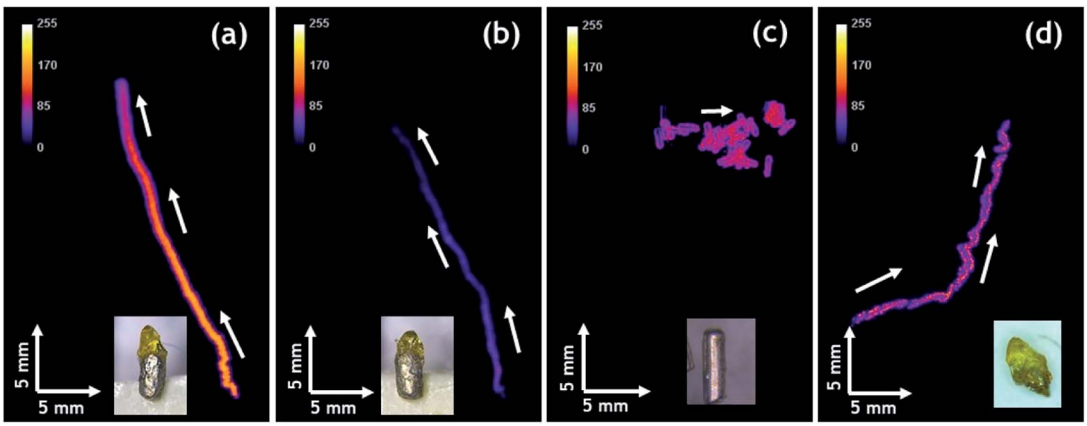

Fig. 3 Tracks of the maximum light intensity of anisotropic Mg swimmers moving at the surface of a 1 mM $Ru(bpy)_3(PF_6)_2$, 20 mM $K_2S_2O_8$, 20 mM H_2SO_4 in H_2O/ACN (1/1) solution; (a) and (b) two different polymer modified anisotropic Mg/EP Janus particles, (c) unmodified anisotropic particle and (d) particle from (a) after five additional experiments. Inset: optical pictures of the anisotropic particles. Global time of every experiment is 90 seconds.

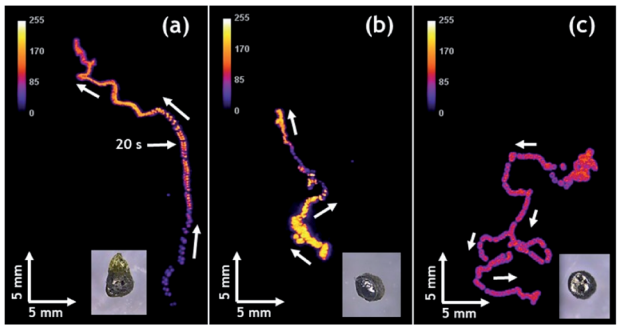

Fig. 4 Tracks of the maximum light intensity of three different initially isotropic particles moving at the surface of a 1 mM $Ru(bpy)_3(PF_6)_2$, 20 mM $K_2S_2O_8$, 20 mM H_2SO_4 in H_2O/ACN (1/1) solution; (a) polymer modified isotropic Mg/EP Janus particle, (b) and (c) unmodified particles. Inset: optical pictures of the particles. Global time of the experiment 90 seconds.

trajectory, which however starts quite rapidly to transform into a more erratic motion (Fig. 4a and Video S2†).

In very strong contrast to this, the unmodified isotropic Mg particles exhibit right from the beginning a pronounced random walk behavior (Fig. 4b and c and Video S3†). However, occasionally the trajectories can also exhibit straight sections, but in an unpredictable way. This can be explained by the adhesion of H_2 bubbles. Once H_2 bubbles attach to the surface of the modified swimmer, further bubble formation becomes asymmetric with respect to the swimmer axis, and can temporarily cause a preferential direction. From all these observations, it becomes evident that the higher the global asymmetry of the swimmer, the better is the directional control. Once again, an evaluation of the straightness index provides a more quantitative evidence. The isotropic Mg/EP Janus particle presents a straightness index of 0.76, whereas, for two different unmodified particles the straightness index decreases to 0.52 and 0.19, respectively (Fig. 4b and c). The latter difference nicely illustrates the fact that the particle of Fig. 4b is not completely spherical, whereas the swimmer of Fig. 4c is perfectly isotropic. In a more general way, it can be deduced once again from Fig. 4, that a decrease in global asymmetry of the swimmers causes a considerable decrease of the straightness index, which translates into a more pronounced random motion (Fig. S3†). Therefore, when combining an initially already anisotropic object with a further increase in asymmetry by depositing the protecting polymer layer, motion is almost perfectly linear ($D/L = 0.97$). For the other cases, a systematic and rational evolution of the trajectory's straightness is observed. The polymer modified isotropic Mg/EP Janus particle has a lower global asymmetry leading to a D/L value of 0.76, followed by the unmodified anisotropic Mg ($D/L = 0.26$) and the unmodified completely isotropic particles ($D/L = 0.19$).

Conclusions

We present a straightforward concept to design asymmetrically modified Mg microparticles and their use as self-propelled chemiluminescent swimmers with predictable trajectories. First, bipolar electromilling has been used to prepare anisotropic and isotropic Mg microparticles. At a constant applied electric field, tuning the initial length of the wires and the duration of electrodissolution allows the elaboration of well-defined Mg microparticles. In a second step, indirect bipolar electrodeposition was used to prepare asymmetrically modified polymer/Mg microparticles. The so-obtained Janus particles have been used as autonomous chemiluminescent swimmers by combining a bubble propulsion mechanism with light emission, triggered by the reductive-oxidation reactions between Mg metal, $Ru(bpy)_3^{2+}$ luminophore and $S_2O_8^{2-}$ co-reactant. Most importantly, it is possible, for the first time, to fine-tune in a rational way the degree of asymmetry of the synthesized particles. The modified particles present a very pronounced directional motion, in comparison with the unmodified specimens, due to a better spatial control of the H_2 bubble formation. The proposed methodology allows changing in a controlled way the degree of global asymmetry of the swimmers, and thus to vary on purpose the directionality of their trajectories. Although this is for the moment a fundamental proof-of-principle study, this type of light emitting swimmers might be interesting for sensing applications, *e.g.*, monitoring the CL quenching in the presence of certain analytes. Finally, the straightforward tracking of motion in real time, enabled by the bright light emission, may facilitate the study of collective behavior such as swarming and schooling,[58] when several of these swimmers are launched simultaneously. This should help to reveal and understand more easily inter-swimmer communication.

Conflicts of interest

There are no conflicts to declare.

Acknowledgements

The project has been funded by the European Research Council (ERC) under the European Union's Horizon 2020 research and innovation program (grant agreement no. 741251, ERC Advanced grant ELECTRA). The authors are very grateful to Camille Colin for his skilful help with the data analysis. ALD acknowledges the University of Bordeaux for her PhD scholarship.

References

1 J. Wang, *Nanomachines: Fundamentals and Applications*, Wiley-VCH, 2013.
2 S. Sanchez, L. Soler and J. Katuri, *Angew. Chem., Int. Ed.*, 2015, **54**, 1414.
3 S. Sengupta, M. E. Ibele and A. Sen, *Angew. Chem., Int. Ed.*, 2012, **51**, 8434.
4 C. W. Shields IV and O. D. Velev, *Chem*, 2017, **3**, 539.
5 J. G. S. Moo, C. C. Mayorga-Martinez, H. Wang, B. Khezri, W. Z. Teo and M. Pumera, *Adv. Funct. Mater.*, 2017, 1604759.
6 W. F. Paxton, S. Sundarajan, T. E. Mallouk and A. Sen, *Angew. Chem., Int. Ed.*, 2006, **45**, 5420.

7 T. E. Mallouk and A. Sen, *Sci. Am.*, 2009, **300**, 72.
8 M. Medina-Sánchez, V. Magdanz, M. Guix, V. M. Fomin and O. G. Schmidt, *Adv. Funct. Mater.*, 2018, **28**, 1707228.
9 S. Palagi, D. P. Singh and P. Fischer, *Adv. Opt. Mater.*, 2019, 1900370.
10 M. Zarei and M. Zarei, *Small*, 2018, 1800912.
11 D. Rojas, B. Jurado-Sanchez and A. Escarpa, *Anal. Chem.*, 2016, **88**, 4153.
12 W. Duan, W. Wang, S. Das, V. Yadav, T. E. Mallouk and A. Sen, *Annu. Rev. Anal. Chem.*, 2015, **8**, 311.
13 T. Patino, A. Porchetta, A. Jannasch, A. Llado, T. Stumpp, E. Schäffer, F. Ricci and S. Sanchez, *Nano Lett.*, 2019, **19**, 3440.
14 D. Kagan, R. Laocharoensuk, M. Zimmerman, C. Clawson, S. Balasubramanian, D. Kang, D. Bishop, S. Sattayasamitsathit, L. Zhang and J. Wang, *Small*, 2010, **6**, 2741.
15 F. Mou, C. Chen, Q. Zhong, Y. Yin, H. Ma and J. Guan, *ACS Appl. Mater. Interfaces*, 2014, **6**, 9897.
16 S. Campuzano, B. Esteban-Fernández de Ávila, P. Yánez-Sedeño, J. M. Pingarrón and J. Wang, *Chem. Sci.*, 2017, **8**, 6750.
17 W. Gao and J. Wang, *ACS Nano*, 2014, **84**, 3170.
18 W. Gao, X. Feng, A. Pei, Y. Gu, J. Li and J. Wang, *Nanoscale*, 2013, **5**, 4696.
19 S. Ebbens and J. R. Howse, *Langmuir*, 2011, **27**, 12293.
20 N. Wolff, V. Ciobanu, M. Enachi, M. Kamp, T. Braniste, V. Duppel, S. Shree, S. Raevschi, M. Medina-Sánchez, R. Adelung, O. G. Schmidt, L. Kienle and I. Tiginyanu, *Small*, 2019, 1905141.
21 L. Bouffier, V. Ravaine, N. Sojic and A. Kuhn, *Curr. Opin. Colloid Interface Sci.*, 2016, **21**, 57.
22 B. Gupta, M. C. Afonso, L. Zhang, C. Ayela, P. Garrigue, B. Goudeau and A. Kuhn, *ChemPhysChem*, 2019, **20**, 941.
23 G. Salinas, A. L. Dauphin, C. Colin, E. Villani, S. Arbault, L. Bouffier and A. Kuhn, *Angew. Chem., Int. Ed.*, 2020, **59**, 7508.
24 R. Sharma and O. D. Velev, *Adv. Funct. Mater.*, 2015, **25**, 5512.
25 J. Roche, S. Carrara, J. Sanchez, J. Lannelongue, G. Loget, L. Bouffier, P. Fischer and A. Kuhn, *Sci. Rep.*, 2014, **4**, 6705.
26 M. Sentic, G. Loget, D. Manojlovic, A. Kuhn and N. Sojic, *Angew. Chem., Int. Ed.*, 2012, **51**, 11284.
27 M. Hesari and Z. Ding, *J. Electrochem. Soc.*, 2016, **163**, H3116.
28 A. J. Bard, *Electrogenerated Chemiluminescence*, Marcel Dekker, 2004.
29 W. Miao, *Chem. Rev.*, 2008, **108**, 2506.
30 E. H. Doeven, G. J. Barbante, C. F. Hogan and P. S. Francis, *ChemPlusChem*, 2015, **80**, 456.
31 M. Sentic, S. Arbault, L. Bouffier, D. Manojlovic, A. Kuhn and N. Sojic, *Chem. Sci.*, 2015, **6**, 4433.
32 G. Loget, D. Zigah, L. Bouffier, N. Sojic and A. Kuhn, *Acc. Chem. Res.*, 2013, **46**, 2513.
33 W. Guo, X. Lin, F. Yan and B. Su, *ChemElectroChem*, 2016, **3**, 480.
34 L. Bouffier, D. Zigah, C. Adam, M. Sentic, Z. Fattah, D. Manojlovic, A. Kuhn and N. Sojic, *ChemElectroChem*, 2014, **1**, 95.
35 M. Sentic, S. Arbault, B. Goudeau, D. Manojlovic, A. Kuhn, L. Bouffier and N. Sojic, *Chem. Commun.*, 2014, **50**, 10202.
36 V. Eßmann, S. Voci, G. Loget, N. Sojic, W. Schuhmann and A. Kuhn, *J. Phys. Chem. Lett.*, 2017, **8**, 4930.
37 A. L. Dauphin, A. Akchach, S. Voci, A. Kuhn, G. Xu, L. Bouffier and N. Sojic, *J. Phys. Chem. Lett.*, 2019, **10**, 5318.
38 A. L. Dauphin, S. Arbault, A. Kuhn, N. Sojic and L. Bouffier, *ChemPhysChem*, 2020, **21**, 600.
39 R. María-Hormigos, A. Escarpa, B. Goudeau, V. Ravaine, A. Perro and A. Kuhn, *Adv. Mater. Interfaces*, 2020, 1902094.
40 S. E. Fosdick, K. N. Knust, K. Scida and R. M. Crooks, *Angew. Chem., Int. Ed.*, 2013, **52**, 10438.
41 C. A. C. Sequeira, D. S. P. Cardoso and M. L. F. Gameiro, *Chem. Eng. Commun.*, 2016, **203**, 1001.
42 L. Koefoed, S. U. Pedersen and K. Daasbjerg, *Curr. Opin. Electrochem.*, 2017, **2**, 13.
43 N. Karimian, P. Hashemi, A. Afkhami and H. Bagheri, *Curr. Opin. Electrochem.*, 2019, **17**, 30.
44 N. Shida, Y. Zhou and S. Inagi, *Acc. Chem. Res.*, 2019, **52**, 2598.
45 Z. A. Fattah, G. Loget, V. Lapeyre, P. Garrigue, C. Warakulwit, J. Limtrakul, L. Bouffier and A. Kuhn, *Electrochim. Acta*, 2011, **56**, 10562.
46 G. Loget, G. Larcade, V. Lapeyre, P. Garrigue, C. Warakulwit, J. Limtrakul, M.-H. Delville, V. Ravaine and A. Kuhn, *Electrochim. Acta*, 2010, **55**, 8116.
47 A. Srinivasan, J. Roche, V. Ravaine and A. Kuhn, *Soft Matter*, 2015, **11**, 3958.
48 Z. A. Fattah, L. Bouffier and A. Kuhn, *Appl. Mater. Today*, 2017, **9**, 259.
49 J. Roche, E. Gianessi and A. Kuhn, *Phys. Chem. Chem. Phys.*, 2014, **16**, 21234.
50 B. Esteban-Fernández de Ávila, P. Angsantikul, J. Li, M. A. Lopez-Ramirez, D. E. Ramírez-Herrera, S. Thamphiwatana, C. Chen, J. Delezuk, R. Samakapiruk, V. Ramez, M. Obonyo, L. Zhang and J. Wang, *Nat. Commun.*, 2017, **8**, 272.
51 C. Chen, E. Karshalev, J. Guan and J. Wang, *Small*, 2018, **14**, 1704252.
52 W. Wang, W. Duan, S. Ahmed, T. E. Mallouk and A. Sen, *Nano Today*, 2013, **8**, 531.
53 G. Loget, J. Roche, E. Gianessi, L. Bouffier and A. Kuhn, *J. Am. Chem. Soc.*, 2012, **134**, 20033.
54 H. S. White and A. J. Bard, *J. Am. Chem. Soc.*, 1982, **104**, 6891.
55 J. Suk, Z. Wu, L. Wang and A. J. Bard, *J. Am. Chem. Soc.*, 2011, **133**, 14675.
56 F. Mou, C. Chen, H. Ma, Y. Yin, Q. Wu and J. Guan, *Angew. Chem., Int. Ed.*, 2013, **52**, 7208.
57 S. Benhamou, *J. Theor. Biol.*, 2004, **229**, 209.
58 W. Wang, W. Duan, S. Ahmed, A. Sen and T. E. Mallouk, *Acc. Chem. Res.*, 2015, **48**, 1938.